Original article

Anna Hojná*, Patricie Halodová, Michal Chocholoušek, Zbyněk Špirit and Lucia Rozumová

Environmentally assisted cracking of T91 ferritic-martensitic steel in heavy liquid metals

https://doi.org/10.1515/corrrev-2019-0035
Received April 12, 2019; accepted November 10, 2019; previously published online January 31, 2020

Abstract: In order to advance material development for future nuclear systems, an insight into the cracking conditions of T91 ferritic-martensitic steel in heavy liquid metals (HLM) is provided. The paper critically reviews previous experimental data and summarizes them with new results. The new testing of T91 steel was performed in contact with slow flow and static HLM to study crack initiation, especially in liquid PbBi eutectic at 300°–350°C and Pb at 400°C with about 1×10^{-6} wt.% of oxygen. Pre-stressed coupons were exposed to the liquid metals for up to 2000 h. Constant extension rate tests (CERTs) were performed in the liquid metals to accelerate cracking development. Under static conditions, the testing resulted in oxidation without any crack observation. Under the CERT ones, the T91 steel showed a tendency to crack initiation in PbBi, while in Pb, cracks were not initiated even when the oxide layer was broken. Moreover, the environmentally assisted crack initiated at the maximum load and continued to grow under further loading without unstable failure. Both previous and new data have confirmed that high stress and plastic strain are pre-conditions for the environmentally assisted cracking of T91 in static HLM. It indicates that in the systems utilizing continuous oxygen control of HLM, the LME/EAC of the T91 could develop only in the beyond design load conditions. Further testing is necessary to address the HLM flow speed effect.

Keywords: environmentally assisted cracking; ferritic-martensitic steel; lead; lead-bismuth eutectic; liquid metal embrittlement.

***Corresponding author: Anna Hojná,** Centrum výzkumu Řež, Řež 130, 25068 Husinec, Czech Republic, e-mail: anna.hojna@cvrez.cz
Patricie Halodová, Michal Chocholoušek, Zbyněk Špirit and Lucia Rozumová: Centrum výzkumu Řež, Řež 130, 25068 Husinec, Czech Republic

Abbreviations

AS	austenitic stainless
BSE	backscattered electron image
CERT	constant extension rate test
DSA	dynamic strain aging
E	Young's modulus, GPa
EAC	environmentally assisted cracking
EDM	electrical discharged machining
F/M	ferritic/martensitic
FIB	focused ion beam
HLM	heavy liquid metal
LBE	eutectic alloy of Pb (44.5%) Bi (55.5%)
LFR	lead fast reactor
LME	liquid metal embrittlement
R0, R2	test extension rate, m/s
SAED	selected-area electron diffraction
SE	secondary electron image
SEM	scanning electron microscope
TEM	transmission electron microscope
UTS	ultimate tensile strength, MPa
YS	yield strength, MPa

1 Introduction

Progress in the development of future nuclear power systems, using the heavy liquid metal (HLM) cooling, is dependent on the availability of structural materials resistant to such operation conditions. For example, the lead-cooled Generation IV fast reactor (LFR) operation requires a long-term resistance of the structural material to a high-flux neutron radiation and to the lead coolant with a wide flow speed range at temperatures of 450°–550°C (Cinotti et al., 2011; Grasso et al., 2014). For the systems using PbBi eutectic (LBE), coolant temperatures up to 450°C are considered (Sapundjiev et al., 2006; SCK · CEN, 2019).

One of the strategies of mitigation of the liquid metal degradation phenomena relies on the use of oxygen injection and continuous control of oxygen concentration in the coolant. It is known that the oxygen concentration in the range from 10^{-7} to 10^{-6} wt.% at 400°–500°C effectively decreases corrosion loss rates by forming a stable protective film (passivating oxide layer) on the surface

of structural materials (Schroer & Konys, 2007; Lapauw et al., 2019). The quality of the oxide layers depends, in general, on the level of oxidation potential of the melt, as well as on the composition and surface condition of the structural materials (Yeliseyeva et al., 2008). The protective film must withstand high flow rates (~1–3 m/s) of the coolant.

Even though the compatibility of the HLM coolant with the materials was studied for more than 20 years, long-term performance of the materials, including their susceptibility to liquid metal embrittlement (LME) and dissolution attack, remains an issue. The HLM degradation issues need to be minimized by proper selection of the structural materials. Generally, the high Cr ferritic/martensitic (F/M) and austenitic stainless (AS) steels were considered to be used as the structural materials for the HLM-cooled power systems. While the F/M steels (e.g. T91, Eurofer, etc.) suffer mainly from the LME at lower temperatures, the AS steels (e.g. 316L, 1.4970, etc.) are prone to the dissolution attack at higher temperatures. The dissolution attack involves (i) dissolution of alloying elements, such as highly soluble Ni and Mn, as well as Cr, (ii) liquid metal penetration into the material, and (iii) ferritization of the dissolution-affected zone due to the removal of the austenite stabilizers, Ni and Mn (Lambrinou et al., 2017; Lapauw et al., 2019).

The steels exposed to liquid PbBi or liquid Pb, containing the required oxygen content, form very thin Cr-based oxide layers that can significantly reduce corrosion rate. The oxide layer can have either a double- or single-layer structure, depending on the original surface, temperature, oxygen concentration, flow rate, and time. The optimal double-layer protective oxide consists of an outer magnetite and inner Cr–Fe spinel layers (Heinzel et al., 2014). Figure 1 summarizes the results of the corrosion exposure tests performed on the AS, and F/M and martensitic steels in LBE containing the required oxygen content at various temperatures, which are available from the literature (Deloffre et al., 2002; Aiello et al., 2004a; Martín et al., 2004; Heinzel et al., 2014; Schroer et al., 2014a,b; Tsisar et al., 2017). General trends can be recognized from the plots: (i) for both types of steels, the tendency to increase the protective oxide layer thickness with increasing temperature of the LBE, and (ii) for F/M and martensitic steels, the increase in the oxide thickness with increased time of exposure, including the tendency to saturation. For the AS steels, owing to the large data scatter, which is likely caused by the dissolution attack, the oxide thickness has not shown any tendency to saturation. The observed stress effect of the F/M steels needs future attention. To be able to draw similar plots for the structural materials used for LFR operation conditions, more corrosion tests would need to be performed in the liquid Pb.

The paper deals with the 9% Cr F/M steel T91, which used to be one of the best candidates for LFR internal structures, owing to its very good strength, toughness, resistance to the radiation, and oxidation/dissolution in HLM. However, suitability of the T91 was questioned due to its indicated sensitivity to cracking in HLM, namely, LBE and Pb, based on data from laboratory testing (Nicaise et al., 2001; Auger et al., 2004; Van den Bosch et al., 2006; Di Gabriele et al., 2008; Long & Dai, 2008; Vogt et al., 2008; Coen et al., 2010; Auger et al., 2011; Gorse et al., 2011; Hojná & Di Gabriele, 2011; Gong et al., 2015; Hojná et al., 2015; Stergar et al., 2016; Di Gabriele et al., 2017).

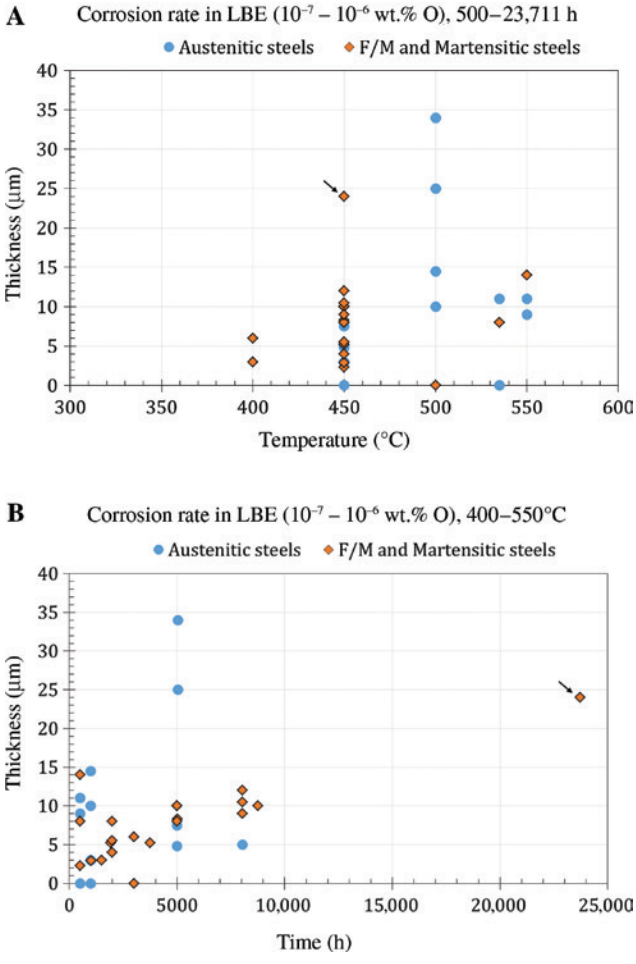

Figure 1: Thicknesses of the oxide layer formed on austenitic [316L (Martín et al., 2004; Heinzel et al., 2014; Schroer et al., 2014b), 304L (Martín et al., 2004), 1.4970 (Heinzel et al., 2014)], F/M (T91, E911 (Aiello et al., 2004a; Schroer et al., 2014a; Tsisar et al., 2017; Yurechko et al., 2018)], and martensitic steels (F82H (Martín et al., 2004), 56T5 (Deloffre et al., 2002)) exposed to LBE as a function of temperature (A) and time (B). The arrow marks the T91 exposed to LBE within creep testing (Yurechko et al., 2018).

This paper is intended to discuss and review the previous conclusions, based on those laboratory tests, and to consider the rehabilitation of the T91 as a suitable candidate.

If possible, the compatibility of the structural materials with the proposed operational conditions should be investigated by applying not only corrosion but corrosion-mechanical testing as well. The testing of materials should preferably address the synergistic effects of the HLM environment with specific oxygen content, flow rate, temperature, and stress up to the levels allowed in operational design. However, in most of the previous studies, performance of the T91 under stress in HLM, namely, in LBE (Auger et al., 2004; Van den Bosch et al., 2006; Di Gabriele et al., 2008; Long & Dai, 2008; Vogt et al., 2008; Coen et al., 2010; Auger et al., 2011; Gorse et al., 2011; Hojná & Di Gabriele, 2011; Gong et al., 2015; Stergar et al., 2016), and also in Pb (Nicaise et al., 2001; Hojná et al., 2015; Di Gabriele et al., 2017) was studied under the out-of-design conditions, i.e. in static HLM containing too low or too high oxygen, and with high stresses and plastic strains applied, and mechanical testing after long-term exposure in dynamic LBE with oxygen content below the design level was also performed (Aiello et al., 2004b). The sensitivity of the T91 to cracking in HLM was detected under these extreme conditions.

The sensitivity to cracking in HLM, associated with typical cleavage-like fracture initiation and growth under applied stress, used to be called liquid metal embrittlement (LME). However, it was recently proved that liquid metal atoms do not diffuse into bulk metal to make it brittle, but only locally penetrate into high-plastic deformed regions (Serre et al., 2018). It means that the cracking can be regarded more accurately as a special case of the environmentally assisted cracking (EAC) – LME/EAC. Although the mechanism of the LME/EAC is not fully understood yet, several arguments seem to point out that adsorption of liquid metal on a bare material surface is the key triggering factor of the process (Lynch, 1988; Martin et al., 2012). Specifically, (i) the sensitivity to cracking uses to be the highest close to the liquid metal melting point (LBE: 127°C, Pb: 328°C), and it decreases with increasing temperature, (ii) wetting is a necessary pre-condition, and (iii) after initiation, the crack propagation is so fast that diffusion is excluded. Moreover, plastic flow seems to be involved in the process, as the LME/EAC occurred in ferritic steels, but not in austenitic steels, likely due to their superior plasticity and their cross-slip ability.

In addition, focused experiments were performed to study characteristics of the LME/EAC crack development in the T91 in HLM under various load conditions. The LME/EAC appeared within low cycle fatigue testing (e.g. Vogt et al., 2008; Gong et al., 2015), but the cases of cracking were difficult to repeat in quasi-static load conditions. It was observed by several authors (Long & Dai, 2008; Van den Bosch et al., 2009; Auger et al., 2011) that the static fracture resistance of the T91 steel in LBE decreased at 200°–300°C by 20–30%, together with a tendency to mix ductile with cleavage-like fracture. Later, the fracture toughness testing was repeated using the LME/EAC cleavage-like preexisting cracks produced by a special procedure (Magielsen et al., 2015), which included a short exposure in the LBE with a very low oxygen content at 450°C, in order to stimulate corrosion attack of the surface. With the cleavage-like pre-crack, the fracture toughness decreased to about 10% of the value measured in air. It is worth noting that the crack development in the T91 steel in HLM within all the tests showed to be a stable growth not leading to rapid failure (Hojná et al., 2016).

To verify the sensitivity of the T91 to the LME/EAC in simulated HLM operational conditions with application of the allowable stresses and oxygen-controlled chemistry, a new type of experiments was performed recently. The testing was focused on studying the LME/EAC crack initiation conditions in static HLM (Duchoň et al., 2018; Hojná et al., 2018a,b,c; Halodová et al., 2019). The sensitivity tests in the dynamic HLM are still to be performed. Moreover, long-term performance of the T91 steel in high-flow HLM with corresponding design oxygen content followed by the crack initiation testing has not been studied yet.

The paper summarizes the key results of the new type of experiments for the T91 steel exposed in two low-flow HLM environments (Pb, PbBi-LBE) as well as the data, which were partially published in previous papers (Duchoň et al., 2018; Hojná et al., 2018a,b,c; Halodová et al., 2019). The conditions for occurrence (initiation) of the LME/EAC in the T91 in contact with the HLM are explained and discussed in the paper.

2 Materials and methods

2.1 Material

The T91 ferritic-martensitic steel (Grade 91 Class 2/S50460), with the chemical composition of 8.895 wt.% Cr, 0.889% Mo, 0.401% Mn, 0.235% Si, 0.121% Ni, 0.202% V, 0.080% Cu, 0.079% Nb, 0.048% N, 0.019% P, 0.010% Al, 0.102% C, bal. Fe, as used in this study, was produced by Industeel, ArcelorMittal group for EC EUROTRANS/DEMETRA project (Van den Bosch, 2009). The material was normalized at 1150°C for 15 min with subsequent

water cooling to room temperature and finally annealed at 770°C for 45 min, then slowly cooled in the air. The material was provided in the form of a 15-mm-thick sheet. The microstructure consisted of the lath martensite with original austenitic grains of 20 μm. The mechanical characteristics: the yield (YS) and the ultimate tensile (UTS) strengths were 503 MPa and 621 MPa, respectively, at 300°C, and 456 MPa and 562 MPa, at 400°C. The Young's modulus (E) of 240 GPa at 300°–350°C and 182 GPa at 400°C was used.

2.2 Specimens

For tests described in the paper, several types of test specimens were used. All the specimen types are listed in Table 1. Besides the two types of specimens, which were used in previous test campaigns (Di Gabriele et al., 2008; Hojná et al., 2015; Di Gabriele et al., 2017), i.e. the smooth and notched tensile bars of 4-mm diameter and 20-mm gauge length, the other two new types used were (1) Flat coupons of 1-mm thickness, 5-mm width, and 22-mm length, manufactured by electrical discharged machining (EDM); the large flat surface was ground up to 500-grid finish, while the sides and edges stayed untreated; (2) flat tapered specimens of 3-mm thickness, 4- to 6.41-mm width and 26-mm gauge length, fabricated by wire cutting using EDM with the longitudinal axis oriented in the rolling direction. Two parallel surfaces were prepared before testing with two different surface finishes: one was ground to 500 grid and the other polished to 1-μm finish using diamond paste; the sides and edges of the specimens stayed untreated.

2.3 Equipment and environment

Static exposure tests were performed in a static tank in liquid Pb at 400°C, and in a convectional flow loop COLONRI I described elsewhere (Hojná et al., 2018c) in LBE at 350°C. The static tank consisted of a stainless-steel autoclave with an inner alumina crucible, which prevented direct contact of the tank walls with the Pb. The oxygen content was maintained at 10^{-7} wt.% using Ar/H_2 gas bubbling and measured using Bi/Bi_2O_3 oxygen sensors.

Mechanical testing was performed using the electromechanical testing machine Z250 (Zwick/Roell, Ulm, Germany) and the HLM system built on the electromechanical creep testing machine Kappa 50DS (Zwick/Roell, Ulm, Germany). The HLM system consisted of two vessels, where the first one was used for heavy liquid metal melting and oxygen setting by Ar/H_2 gas bubbling, and the second one was used for the specimen loading. The oxygen content was measured in both vessels using Bi/Bi_2O_3 oxygen sensors. The oxygen content of about 1×10^{-6} wt.% was maintained in Pb/PbBi by gas bubbling. The specimen, fixed into grips, was exposed for 1 day before loading start, in order to stabilize the oxygen concentration.

2.4 Test methods

For static exposure, the flat coupon was pre-loaded in a test holder by a three-point bent to deflection y calculated according to ISO 7539-2 standard: $y=\sigma\times H^2/(6\times E\times t)$, where σ is the applied stress at test temperature, H is the span, E is the Young's modulus, and t is the coupon thickness. The pre-stress of 100% to 130% of YS was applied. The holder was then inserted into the static tank or the COLONRI I loop.

For slow tensile loadings, the constant extension rate test (CERT) was applied using several extension rates from 2×10^{-8} to 2×10^{-4} m/s, corresponding to strain rates from 1×10^{-6} to 1×10^{-2} s^{-1} (at the minimum cross section of the tapered specimen). The first specimen was loaded up to rupture; other tests were stopped after the maximum load.

2.5 Post-test investigation

After exposure, the surface was at first observed by scanning electron microscope (SEM). Then, cross and

Table 1: Summary of all types of test specimens discussed in this paper.

Designation	Specimen type	Loading	Displacement rate	References
Bend	Flat coupon	Three-point bend	Static	This paper, Hojná et al., 2018a,b,c
Notch	Notched round bar	Tensile	Slow, quasi-static	Hojná et al., 2015; Di Gabriele et al., 2017
Smooth	Smooth round bar	Tensile	Slow, quasi-static	Di Gabriele et al., 2008; Hojná et al., 2015; Di Gabriele et al., 2017
Tapered	Flat tapered platelet	Tensile	Slow, quasi-static (R0, R2)	This paper, Hojná et al., 2018a,b

longitudinal section samples were prepared for further investigation. If necessary, the remaining Pb/PbBi was removed through immersing of the specimen in a solution of H_2O_2, CH_3COOH, and CH_3CH_2OH in the 1:1:1 ratio. The observation and analyses were performed using MIRA3 GMU SEM and a dual-beam FIB-SEM system LYRA3 GMU (TESCAN, Brno, Czech Republic).

3 Results

3.1 Static exposure tests

Tests were performed with the coupons pre-stressed and then exposed to PbBi (LBE) at 350°C for 500, 1000, and 2000 h or to Pb at 400°C for 500 and 1000 h. Based on previous experience, it was expected that the pre-stress would undergo relaxation up to 20% with time and temperature.

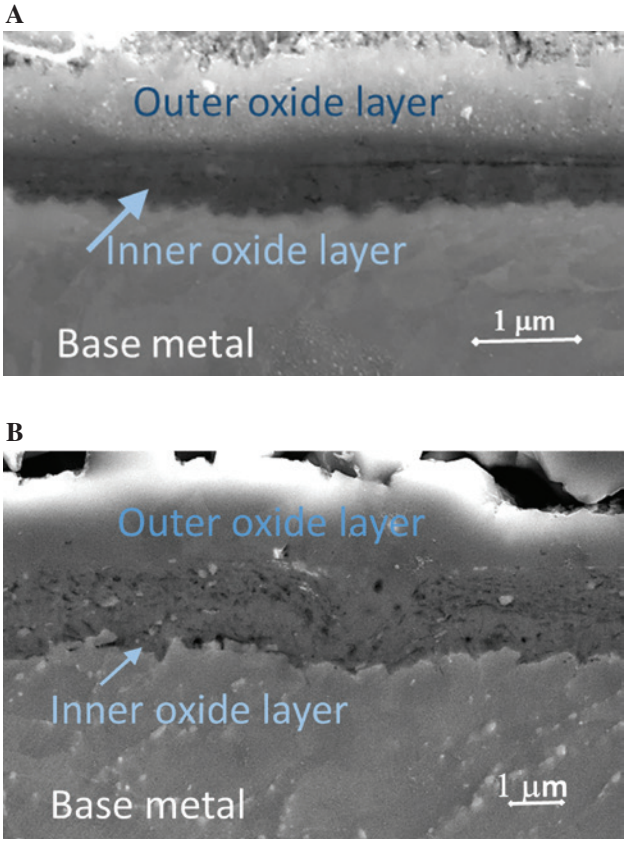

Figure 2: Double-layer oxide scale developed under 120% YS pre-stress during 1000 h in (A) PbBi at 350°C and (B) Pb at 400°C; SEM SE images.

In PbBi: Steel surface that was in contact with LBE covered with thin continuous oxide scale, which appeared as a dark-gray dull layer on the surface. The oxidized surface consisted of Fe–O layer grown outward on top of the Fe–Cr-rich spinel grown inward the steel. The thickness of the oxide was ~1.5 µm after 500 h and ~2 µm after 1000 and more hours. The thickness and character of the oxides were found to be slightly influenced by stress. In locations of the highest tension, variations in thickness and wavy character of the interface line between the inner oxidation zone and the matrix could be observed (Figure 2A). However, no tendency to an oxide failure was detected. Consequently, no LME/EAC crack was observed in any of the bend coupons.

Detailed transmission electron microscopy (TEM) observation was performed on an FIB lamella cut from the specimen exposed for 2000 h in LBE (Duchoň et al., 2018). The outer oxide layer was identified by SAED (selected-area electron diffraction) as magnetite, and the inner layer was identified as the Fe–Cr spinel. The TEM revealed impurities present within the oxide layers – particles of $Cr_{23}C_6$ in spinel and Pb (Pb-Bi) clusters in magnetite. The interface between the oxide layers was highly visible in SEM due to a change in SE/BSE contrast and appearance (Figure 2A). The less compact Fe–Cr spinel layer contained many pores. Several larger pores appeared on the magnetite/spinel interface.

In Pb: The surface after the 1000-h exposure and subsequent chemical cleaning from Pb showed areas of non-continuous and continuous oxide layer distribution. The oxide exhibited a double-layer structure (Figure 2B). The thickness range varied from about 1.5 to 5 µm for non-pre-stressed specimens as well as for the pre-stressed ones. Besides local changes in the size of the oxide layer, no tendency either to disrupt the oxide scale or to initiate cracks was observed. The outer layer consisted of Fe–O without Pb clusters. The inner layer was a Fe–Cr spinel that was very porous. The difference in compactness of the inner Fe–Cr spinel layer and the outer magnetite layer can be seen from the SEM image in Figure 2B.

3.2 Constant extension rate tests

The CERTs were performed with tapered specimens in PbBi (LBE) at 300°C and in Pb at 400°C, using two test rates, and reference testing was in air. The tapered specimen had an advantage that a range of stresses was applied along the gauge length at a single load, so that for each

crack, the stress needed for its formation could be approximately determined. The stress-strain rate data were specific to each cross section. To interpret the test recordings, the force response of the specimen versus the applied displacement should be normally used. However, the dimensions of the specimen differed by about ±0.2 mm due to manual sample preparation by surface grinding and polishing, which would induce a slight distortion of the lines. Therefore, the test recordings are shown here in a plot of the engineering stress corresponding to the minimum cross section, respecting the real dimensions (Figure 3).

In air, at both test temperatures, the maximum stress was lower for the faster test rate R0 than for the slower test rate R2. Moreover, the test curves of the R2 showed distinctive oscillations. These observations were indicative of the dynamic strain aging (DSA) phenomena affecting T91 mechanical behavior at the given conditions. All the test curves measured in HLM showed lower maximum stress than the curves measured in air at 300°C and 400°C, respectively. Moreover, the oscillations were again clearly visible only at the R2 curves. In Figure 3A, the difference of the maximum stresses in air and in PbBi was small, about 40 MPa. In Figure 3B, the difference between the maximum stress in air and in Pb was distinctive, about 60 MPa.

After the CERTs, protective oxide formation was observed on the surface. The double-layer oxide (Figure 4A) was broken in the most strained regions. Thicker oxide was found in 400°C in Pb (Figure 4B) than in 300°C in LBE. The thicker outer layer in Pb tended to peel up when formed on the surface (see Figure 6A).

Several morphologies of cracks appeared on the surface of tapered specimens after CERTs. These cracks, (i) ductile within the slip bands, (ii) broken particles, and (iii) cracks initiating from the specimen edge, were observed in air as well as in HLM. Other types of cracks appeared only on the specimens tested in HLM (Figures 5 and 6).

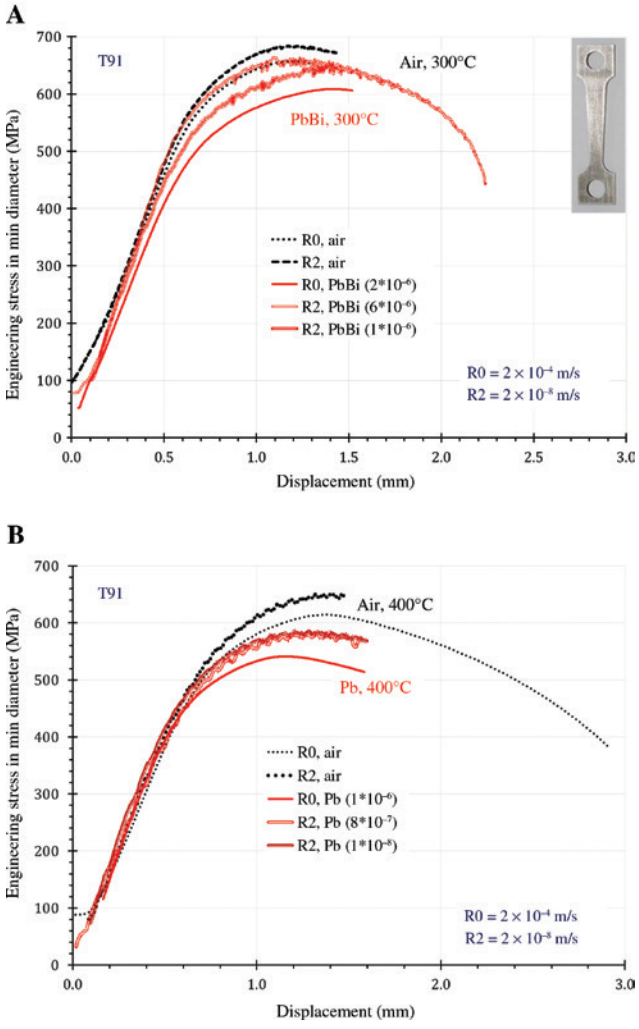

Figure 3: Engineering stress in the minimal cross section versus displacement curves of CERTs of the tapered specimens in air and in the liquid metals: (A) at 300°C and (B) at 400°C; dashed lines stand for air, full lines stand for HLM. The number in brackets stands for oxygen content in wt.%. Photo of the tapered specimen of the minimum diameter 3 × 4 mm is included.

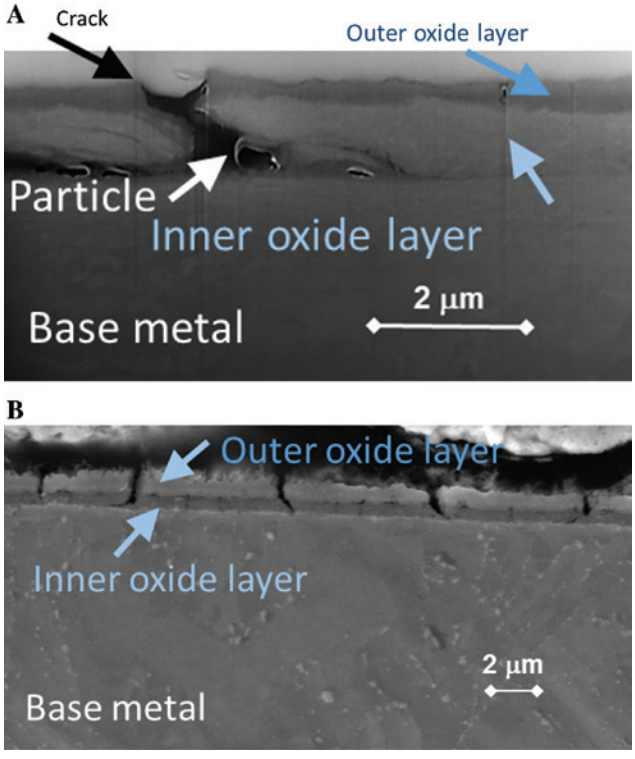

Figure 4: Double-layer oxide scale developed and braked under CERT in (A) LBE at 300°C showing a short crack through the oxide reaching a particle, (B) Pb at 400°C showing many superficial cracks in the oxide; SEM SE images.

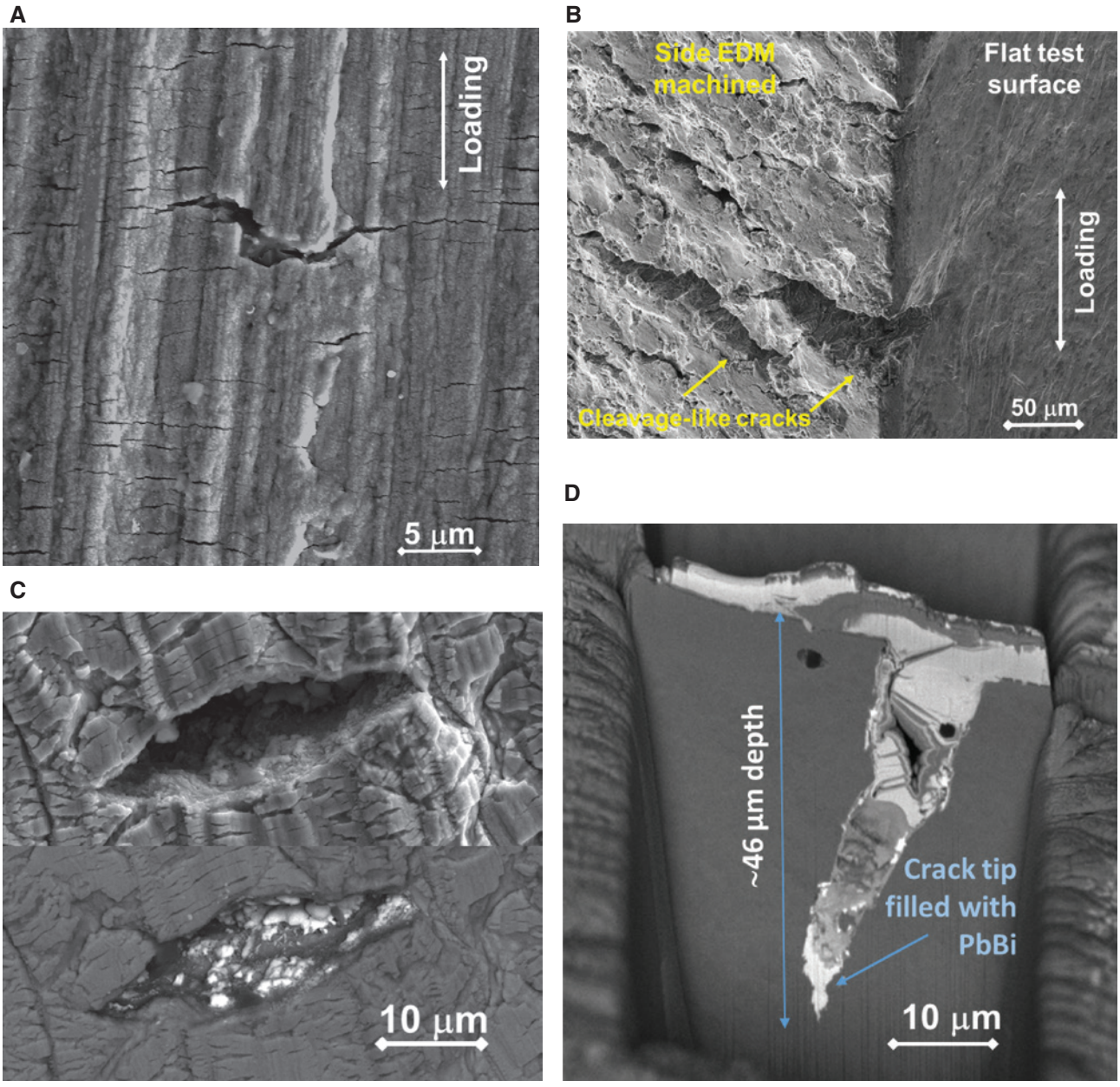

Figure 5: Ground surface of R2-loaded specimen of CERT in LBE and 300°C: (A) the oxide layer with many fine cracks and one larger crack initiating from a subsurface particle; (B) LME/EAC cleavage-like cracks initiating from untreated side and edge of the specimen; (C) BSE image on the bottom showing the open LME/EAC crack, in which the inside contains the remaining LBE and SE image on the top showing many fine cracks in oxide; (D) FIB cut of the open LME/EAC crack of (C) revealing the 46 μm depth (BSE image).

Fine shallow cracks arranged in clusters were observed in LBE (Figure 5A) and also in Pb (Figure 6A). Moreover in LBE, several cleavage-like cracks initiated from the specimen edges (Figure 5B), and few open cracks perpendicular to the load axis appeared on the flat surface (Figure 5C and D). Besides the cracks from the particles, all other cracks were observed only in the plastic strained regions of the specimens. The open cracks, which were identified as the true LME/EAC ones, appeared only in the highest plastic strain regions. The crack position indicated that the crack could be initiated only with the high plastic strain assistance.

Unlike in PbBi, only the shallow cracks within the oxide appeared in all CERT tests in liquid Pb indicating the environmental effect (Figure 6). The crack depth was limited to the outer oxide layer as confirmed in cross sections. The number of the superficial cracks (Figures 5B and 6A) was higher in the faster CERT than in the slower one, where only several cracks appeared on the oxidized surface (Figure 6B).

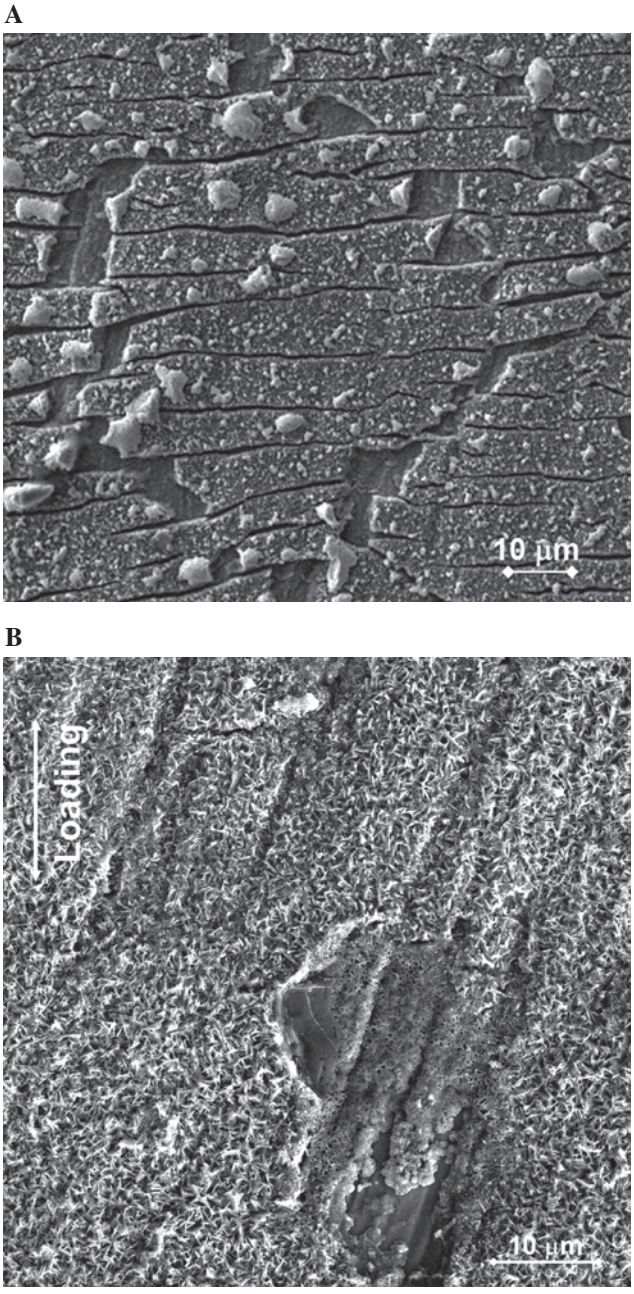

Figure 6: Ground surface after CERT in Pb and 400°C: (A) appearance of the high-strained region surface of R0-loaded tapered specimen showing thick oxide, partly peeled up, and plenty of superficial cracks initiating perpendicular to loading; (B) appearance of the same region of R2-loaded specimen showing mostly continuous oxide with sporadic fine cracks.

4 Discussion

These static and slow loading experiments were performed with the intention to simulate range of operation conditions of the future HLM cooled power systems excluding flow, from static loading corresponding to steady operation to slow loadings corresponding to startups or shutdowns. The test conditions, namely, the static load, were different from most of the previous tests, which, in fact, simulated only emergency operation of the systems.

The experiments showed that the applied stress-strain and the strain rate significantly influenced the LME/EAC damage development in the T91 steel. In static long-term tests performed in both HLMs, no tendency to cracking was found at pre-stress levels about YS (considering a stress relaxation with time and with increasing temperature). It was likely due to stability of the oxide layers, which did not break under the conditions and thus prevented direct contact of the liquid metals with bare metal.

On the other hand, when using the quasi-static strain rates, some cracks were initiated on the surface of tapered specimens in air and HLM. These cracks were sorted into several types. Two crack types appearing only in LBE were observed as LME/EAC: (i) the edge cracks recognized owing to their cleavage-like surface morphology; and (ii) few open cracks that occurred in the region of maximum plastic strain and stress. The depth of the one of the open cracks (Figure 6D) was measured using FIB, as referred elsewhere (Halodová et al., 2019). The crack size was 46 µm in depth, but only about 20 µm on the surface. The open crack filled with PbBi had transgranular and partly inter-lath path typical for the LME/EAC, which concurred with the other cases referred elsewhere (Martin et al., 2012). Thereby, the sensitivity of the T91 to LME/EAC in LBE at the high stress-strain conditions was confirmed. In liquid Pb, such LME/EAC cracks did not initiate even if maximum load was applied on the flat tapered specimen surface. The result was in agreement with previous experience (Di Gabriele et al., 2017) showing the LME/EAC in the T91 in Pb initiating only from notches on tensile specimens loaded over maximum. In order to initiate LME/EAC crack in the T91 in liquid Pb, the stress concentration and nominal stress close to the ultimate strength conditions had to be applied.

Moreover, the shallow cracks in the protective oxide, which appeared in LBE and also in Pb if the faster rate was applied, also had the orientation perpendicular to applied load as typical for environmentally induced cracks. However, from the observation in cross sections, it was found that these cracks were limited only to the oxide layer and did not propagate into the matrix (Figure 4B). These cracks might be attributed to LME/EAC, but only as precursors for the cracking. The oxide layer barrier would have to be broken to open a path for HLM to penetrate to the bare surface to wet it before the LME/EAC could initiate.

At the same time, temperature and strain rate effects appeared in the CERTs with tapered specimens in the two HLM environments. Figure 3 shows that the maximum

stress increased with decreasing test rate from R0 to R2, and oscillations appeared for R2 in air as well as in HLM. These features typically characterized the DSA activity, which is linked to interaction between diffusing solute atoms (C, N interstitial or Cr, Mo substitutional) and moving dislocations (Keller et al., 2012; Zhou et al., 2016). Based on the references, it seems that diffusion of the C, N interstitial atoms could be considered for the DSA (Zhou et al., 2016) at 300°C, but at 400°C, it would be rather the diffusion of the Cr, Mo substitutional atoms (Keller et al., 2012). At 300°C and 400°C, the test curves obtained in air and in LBE/Pb showed about the same drop of the maximum stress with the R2 to R0 change, as well as the similar oscillations that appeared in the R2 curves (Figure 3). It indicates that the DSA activity was not affected by the contact with the HLM environments.

In addition, the temperature effect on the maximum stress appeared stronger in HLM than in air (Figure 3). This effect might point out to other environmental effects in synergy with applied straining. It was not quite clear which physical process could explain the observation. A similar effect was observed in our previous project using tensile tests with smooth bar specimens (Hojná et al., 2015). The specimens tested at 350°–400°C with the R2 strain rate showed higher elongation in liquid Pb than in air. In the previous paper(Hojná et al., 2015), a possible contribution of dislocation creep appearing in Pb at lower temperatures than in air was speculated about (Jianu et al., 2009). The effect might have been a consequence of facilitated diffusion of Cr atoms resulting from surface oxidation. However, this effect was likely small at all studied temperatures. In agreement with previous studies, it was shown that the thin double layer oxides grow at the T91 surface in the liquid metals at the applied test conditions. The oxidation process involved the outward migration of iron and chromium from the steel to the external interface and penetration of oxygen from the liquid metal to the steel/oxide interface. The process left an excess of vacancies inside the steel, and a Cr-depleted zone might have been formed under the inner oxide/metal interface. However, no Cr-depleted zone was observed at the specimens exposed to HLM at 300°–400°C as referred to in the paper. Further testing is needed to explain this observation.

It would be worth evaluating the conditions of LME/EAC initiation (stress, strain, strain rate) of the T91 in HLM applied in the previous and new type of experiments. In summary, the LME/EAC of the T91 was observed at 200°–350°C in LBE and at 350°–400°C in Pb by various authors (Lynch, 1988; Nicaise et al., 2001; Auger et al., 2004; Van den Bosch et al., 2006; Di Gabriele et al., 2008; Long & Dai, 2008; Vogt et al., 2008; Van den Bosch et al., 2009; Coen et al., 2010; Auger et al., 2011; Gorse et al., 2011; Hojná & Di Gabriele, 2011; Martin et al., 2012; Gong et al., 2015; Hojná et al., 2015; Magielsen et al., 2015; Hojná et al., 2016; Stergar et al., 2016; Di Gabriele et al., 2017; Hojná et al., 2018a,b,c; Serre et al., 2018). Most of the earlier papers evaluated the sensitivity from test specimen rupture, but did not specify the conditions of the LME/EAC initiation. Using some of the data, the conditions can be evaluated retrospectively; the new tests describe the conditions directly.

The two graphs in Figure 7 summarize the LME/EAC crack initiation cases plotted into corresponding test conditions applied on the T91 in the two HLM environments,

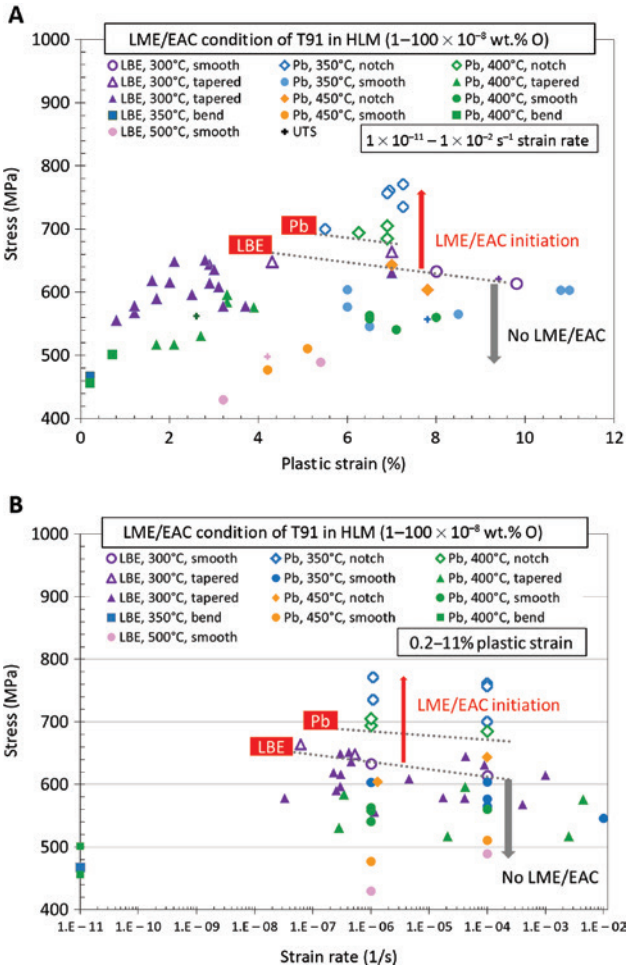

Figure 7: Summary conditions of the T91 (a single batch) testing in Pb at 350°–450°C and PbBi (LBE) at 300°–500°C. The data points (this paper; Di Gabriele et al., 2008; Hojná et al., 2015; Di Gabriele et al., 2017; Hojná et al., 2018a,b,c) indicating yes/no cracking are divided in two graphs: (A) stress versus plastic strain and (B) stress versus strain rate. Smooth, notch, tapered, and bend mean specimen types, which are specified in Table 1. Open points stand for LME/EAC occurrence; full points stand for no cracking; the crosses are colored according to temperature stand for the UTS. The dashed lines mark the threshold stress in Pb and LBE.

which are referred to in this paper and in the previous ones (Di Gabriele et al., 2008; Hojná et al., 2015; Di Gabriele et al., 2017; Hojná et al., 2018a,b,c). The first graph shows the initiation data in the plot of applied stress versus strain, the second one in the plot of stress versus strain rate. The dashed line marks the LME/EAC threshold stress estimated in liquid Pb and LBE.

Overall, plastic strain higher than 4% and existing stress higher than 600 MPa are determining the crack initiation conditions in the static LBE at 300°–350°C and strain rate of $10^{-11} – 10^{-2}$ s^{-1}. That the stress-strain over the UTS exceeds every design conditions of expected component operation. In liquid Pb, at 350°–400°C and at strain rates of $10^{-11} – 10^{-2}$ s^{-1}, the plastic strain higher than 5% and the stress higher than 640 MPa define the LME/EAC initiation. Considering the results, it can be concluded that there is no risk of LME/EAC occurrence under usual design conditions allowing only elastic stresses. On the other hand, the LME/EAC can develop from sharp notches in very high loads overcoming design load of components.

It should be noted, that all the mentioned corrosion-mechanical tests were performed in slow flow or static HLM conditions. Yet, the full rehabilitation of the T91 cannot be inferred on the basis of these results. Further testing of the T91 steel long-term performance is needed to be performed in both HLMs with high flow rate of about 1–3 m/s corresponding to the dynamic operational conditions. It could be expected that the oxide film will develop differently in the high flow conditions, which could probably affect the T91 resistance and, hence, the sensitivity to LME/EAC crack initiation.

5 Conclusions

The current paper brings a new perspective to the phenomenon of LME of the F/M steel T91 in two HLMs, Pb and LBE. The experimental data of LME/EAC sensitivity testing of the T91 in the HLMs are re-assessed. The older type of the sensitivity testing, which resulted in overestimation of T91 sensitivity in HLM is critically discussed, and the new type of the testing based on observation of the crack initiation is introduced. This consists in a series of static and constant extension rate tests at slow strain rates.

Based on the new and previous test results, the following conclusions can be drawn:

1. The T91 shows a tendency to LME/EAC crack initiation in contact with static liquid LBE of 300°C at the conditions of the stress of around UTS together with the high plastic deformation. After initiation, the crack propagates sub-critically and does not lead to an unstable failure.
2. The LME/EAC crack initiation stress and strain conditions in static HLM containing an oxygen concentration of 10^{-7}–10^{-6} wt.% were evaluated. The T91 steel appeared to be resistant to LME/EAC in liquid Pb at 350°–450°C and in LBE at 300°–500°C with applied elastic stresses up to the ultimate tensile strength.

The new testing and its evaluation can be used to partly rehabilitate the T91 steel from the risk of its LME/EAC cracking. It can be concluded that the LME/EAC of the T91 can develop only in the beyond design load conditions if the effect of the HLM flow speed is not taken into account. Further testing is necessary to assess the flow effect.

Funding: This work was supported by the Czech Science Foundation (GAČR) project no. 16-15008S, Funder Id: http://dx.doi.org/10.13039/501100001824. This work was realized within the SUSEN Project (established in the framework of the European Regional Development Fund (ERDF) in project CZ.1.05/2.1.00/03.0108 and of the European Strategy Forum on Research Infrastructures (ESFRI) in the project CZ.02.1.01/0.0/0.0/15_008/0000293, which is financially supported by the Ministry of Education, Youth and Sports – project LM2015093 Infrastructure SUSEN.

Conflict of interest statement: The authors declare no conflict of interests.

References

Aiello A, Azzati M, Benamati G, Gessi A, Long B, Scaddozzo G. Corrosion behaviour of stainless steels in flowing LBE at low and high oxygen concentration. J Nucl Mater 2004a; 335: 169–173.

Aiello A, Agostini M, Benamati G, Long B, Scaddozzo G. Mechanical properties of martensitic steels after exposure to flowing liquid metals. J Nucl Mater 2004b; 335: 217–221.

Auger T, Gorse D, Hamouche-Hadjem Z, Van den Bosch J, Coen G, Almazouzi A, Hojna A, Dalikova K, Di Gabriele F, Serrano M, Gessi A, Agostini P, Vogt J-B, Serre I. Fracture mechanics behaviour of the T91 martensitic steel in contact with liquid lead-bismuth eutectic for application in an accelerator driven system. J Nucl Mater 2011; 415: 293–301.

Auger T, Lorang G, Guérin S, Pastol J-L, Gorse D. Effect of contact conditions on embrittlement of T91 steel by lead–bismuth. J Nucl Mater 2004; 335: 227–231.

Cinotti L, Smith CF, Sekimoto H, Mansani L, Reale M, Sienickie JJ. Lead-cooled system design and challenges in the frame of Generation IV International Forum. J Nucl Mater 2011; 415: 245–253.

Coen G, Van den Bosch J, Almazouzi A, Degrieck J. Investigation of the effect of lead–bismuth eutectic on the fracture properties of T91 and 316L. J Nucl Mater 2010; 398: 122–128.

Deloffre Ph, Terlain A, Barbier F. Corrosion and deposition of ferrous alloys in molten lead–bismuth. J Nucl Mater 2002; 301: 35–39.
Di Gabriele F, Doubkova A, Hojna A. Investigation of the sensitivity to EAC of steel T91 in contact with liquid LBE. J Nucl Mater 2008; 376: 307–311.
Di Gabriele F, Hojná A, Chocholousek M, Klecka J. Behavior of the steel T91 under multi axial loading in contact with liquid and solid Pb. Metals 2017; 7: 342–356.
Duchoň J, Halodová P, Lorinčík J, Di Gabriele F, Hojná A. Characterisation of oxides by advanced techniques. Acta Metallurgica Slovaca 2018; 24: 13–19.
Grasso G, Petrovich C, Mattioli D, Artioli C, Sciora P, Gugiu D, Bandini G, Bubelis E, Mikityuk K. The core design of ALFRED, a demonstrator for the European lead-cooled reactors. Nucl Eng Des 2014; 278: 287–301.
Gong X, Marmy P, Verlinden B, Wevers M, Seefeldt M. Low cycle fatigue behavior of a modified 9Cr–1Mo ferritic–martensitic steel in lead–bismuth eutectic at 350°C – effects of oxygen concentration in the liquid metal and strain rate. Corros Sci 2015; 94: 377–391.
Gorse D, Auger T, Vogt J-B, Serre I, Weisenburger A, Gessi A, Agostini P, Faziod C, Hojna A, Di Gabriele F, Van den Bosch J, Coen G, Almazouzi A, Serrano M. Influence of liquid lead and lead-bismuth eutectic on tensile, fatigue and creep properties of ferritic/martensitic and austenitic steels for transmutation systems. J Nucl Mater 2011; 415: 284–292.
Halodová P, Lorinčík J, Hojná A. Microstructural investigation of LME crack initiated in ferritic/martensitic steel T91 loaded in liquid lead-bismuth eutectic at 300°C. Materials 2019; 12: 38.
Heinzel A, Weisenburger A, Müller G. Corrosion behavior of austenitic steels in liquid lead bismuth containing 10–6 wt.% and 10 – 8 wt.% oxygen at 400–500°C. J Nucl Mater 2014; 448: 163–171.
Hojná A, Di Gabriele F. On the kinetics of LME for the ferritic martensitic steel T91 immersed in liquid PbBi eutectic. J Nucl Mater 2011; 413: 21–29.
Hojná A, Di Gabriele F, Klečka J, Burda J. Behaviour of the steel T91 under uniaxial and multiaxial slow loading in contact with liquid Pb. J Nucl Mater 2015; 466: 292–301.
Hojná A, Di Gabriele F, Klečka J. Characteristics and liquid metal embrittlement of the steel T91 in contact with lead-bismuth eutectic. J Nucl Mater 2016; 472: 163–170.
Hojná A, Di Gabriele F, Chocholoušek M, Halodová P, Lorinčík J. Initiation of LME crack in ferritic martensitic steel in liquid lead-bismuth. J Nucl Mater 2018a; 511: 459–472.
Hojná A, Di Gabriele F, Chocholoušek M, Rozumová L, Vít J. Effect of applied stress on T91 steel performance in liquid lead at 400°C. Materials 2018b; 11: 1–17.
Hojná A, Hadraba H, Di Gabriele F, Husák R. Behaviour of pre-stressed T91 and ODS steels exposed to liquid lead-bismuth eutectic. Corros Sci 2018c; 131: 264–277.
Jianu A, Müller G, Weisenburger A, Heinzel A, Fazio C, Markov VG, Kashtanov AD. Creep-to-rupture tests of T91 steel in flowing Pb–Bi eutectic melt at 550°C. J Nucl Mater 2009; 394: 102–108.
Keller C, Margulies MM, Guillot I. Experimental analysis of the dynamic strain ageing for a modified T91 martensitic steel. Mater Sci Eng. A 2012; 536: 273–275.
Lambrinou K, Charalampopoulou E, Van der Donck T, Delville R, Schryvers D. Dissolution corrosion of 316L austenitic stainless steels in contact with static liquid lead-bismuth eutectic (LBE) at 500°C. J Nucl Mater 2017; 490: 9–27.
Lapauw T, Tunca B, Joris J, Jianu A, Fetzer R, Weisenburger A, Vleugel J, Lambrinou K. Interaction of M_{n+1} AX_n phases with oxygen-poor, static and fast-flowing liquid lead-bismuth eutectic. J Nucl Mater 2019; 520: 258–272.
Long B, Dai Y. Investigation of LBE embrittlement effects on the fracture properties of T91. J Nucl Mater 2008; 376: 341–345.
Lynch SP. Environmentally assisted cracking: overview of evidence for an adsorption-induced localised-slip process. Acta Metallurgica 1988; 36: 2639–2661.
Magielsen L, van Staveren TO, Lambrinou K. Deliverable 3.5: "Guidelines, results and evaluations for fracture toughness tests", MATTER (Materials Testing And Rules), in: Collaborative Project co-funded by the European Commission under the Euratom Research and Training Programme on Nuclear Energy Within the Seventh Framework Programme, Grant Agreement no. 269706. 2015.
Martín FJ, Soler L, Hernández F, Gómez-Briceño D. Oxide layer stability in lead–bismuth at high temperature. J Nucl Mater 2004; 335: 194–198.
Martin ML, Auger T, Johnson DD, Robertson IM. Liquid–metal-induced fracture mode of martensitic T91 steels. J Nucl Mater 2012; 426: 71–77.
Nicaise G, Legris A, Vogt JB, Foct J. Embrittlement of the martensitic steel 91 tested in liquid lead. J Nucl Mater 2001; 296: 256–264.
Sapundjiev D, Al Mazouzi A, Van Dyck S. A study of the neutron irradiation effects on the susceptibility to embrittlement of A316L and T91 steels in lead–bismuth eutectic. J Nucl Mater 2006; 356: 229–236.
SCK · CEN. 2019. MYRRHA: an innovative research installation. Retrieved from: http://sckcen.be/en/Technology_future/MYRRHA
Serre IP, Vogt J-B, Nuns N. TOF-SIMS investigation of absorption of lead and bismuth in T91 steel deformed in liquid lead bismuth eutectic. Appl Surf Sci 2018; 471: 36–42.
Schroer C, Konys J. Physical chemistry of corrosion and oxygen control in liquid lead and lead-bismuth eutectic. Forschungszentrum Karlsruhe 2007; FZKA 7364: ISSN 0947-8620.
Schroer C, Wedemeyer O, Novotny J, Skrypnik A, Konys J. Performance of 9% Cr steels in flowing lead-bismuth eutectic at 450 and 550°C, and 10 – 6 mass% dissolved oxygen. Nucl Eng Des 2014a; 280: 661–672.
Schroer C, Wedemeyer O, Novotny J, Skrypnik A, Konys J. Selective leaching of nickel and chromium from Type 316 austenitic steel in oxygen-containing lead–bismuth eutectic (LBE). Corros Sci 2014b; 84: 113–124.
Stergar E, Eremin SG, Gavrilov S, Lambrecht M, Makarov O, Iakovlev V. Influence of LBE long term exposure and simultaneous fast neutron irradiation on the mechanical properties of T91 and 316L. J Nucl Mater 2016; 473: 28–34.
Tsisar V, Schroer C, Wedemeyer O, Skrypnik A, Konys J. Characterization of corrosion phenomena and kinetics on T91 ferritic/martensitic steel exposed at 450 and 550°C to flowing Pb-Bi eutectic with 10 – 7 mass% dissolved oxygen. J Nucl Mater 2017; 494: 422–438.
Van den Bosch J. ADS candidate materials compatibility with liquid metals in a neutron irradiation environment. PhD thesis, University of Gent, Gent, Belgium, 2009.

Van den Bosch J, Sapundjiev D, Almazouzi A. Effects of temperature and strain rate on the mechanical properties of T91 material tested in liquid lead bismuth eutectic. J Nucl Mater 2006; 356: 237–246.

Van den Bosch J, Coen G, Almazouzi A, Degrieck J. Fracture toughness assessment of ferritic-martensitic steel in liquid lead-bismuth eutectic. J Nucl Mater 2009; 385: 250–257.

Vogt J-B, Verleene A, Serre I, Legris A. Mechanical behaviour of the T91martensitic steel under monotonic and cyclic stressing in liquid metals. J Nucl Mater 2008; 335: 222–226.

Yeliseyeva O, Tsisar V, Benamati G. Influence of temperature on the interaction mode of T91 and AISI 316L steels with Pb–Bi melt saturated by oxygen. Corros Sci 2008; 50: 1672–1683.

Yurechko M, Schroer C, Skrypnik A, Wedemeyer O, Tsisar V, Konys J. Steel T91 subjected to static stress in lead-bismuth eutectic at 450–550 °C and low oxygen concentration. J Nucl Mater 2018; 512: 423–439.

Zhou H, Fang J, Chen Y, Yang L, Zhanga H, Lua Y, Hea Y. Internal friction studies on dynamic strain aging in P91 ferritic steel. Mater Sci Eng A 2016; 676: 361–365.